Interference Filters for Thermophotovoltaic Applications

John Les – Lockheed Martin/Knolls Atomic Power Laboratory

Mathematical Problems in Industry, Delaware, June 1999

(Draft Date: November 2, 1999)

Thomas Borne, Computations and Analysis
Danielle Cross, Rensselær Polytechnic Institute
Gang Du, Rensselær Polytechnic Institute
David A. Edwards, University of Delaware
Joe Haus, The University of Dayton
John King, University of Nottingham
Andrew Lacey, Heriot-Watt University
Peter Monk, University of Delaware
Colin Please, University of Southampton
Hoa Tran, New Jersey Institute of Technology

1   The Problem

The overall intention is to use a source of black-body radiation, perhaps some object being heated inside by burning fuel, to produce electricity from a thermophotovoltaic (TPV) cell by the correct sort of radiation arriving at the cell. Only light below a certain wavelength λ_g will generate a voltage in the cell; such high-frequency radiation may be termed "useful" in contrast to the "useless" lower-frequency radiation. To increase efficiency, ideally the otherwise useless long-wavelength light is returned to the radiator by reflecting back from the TPV cell.

A key part of the device currently under investigation is an "interference filter". This consists of a large number (say around 60) of thin layers (the whole device is about $2\,\mu$m thick) with differing refractive indices. The combination of multiple reflections and refractions, with associated change of phase, results in interference so that light of certain frequencies is mostly reflected back while other light is mostly transmitted through to the other side of the filter (see Section 2). In the ideal case, all the good frequencies will pass through the filter to the TPV cell lying behind it while the bad ones are reflected away (see Fig. 1):

overall reflection coefficient (by power) = 1 for $\lambda < \lambda_g$, 0 for $\lambda > \lambda_g$;

overall transmission coefficient (by power) = 0 for $\lambda < \lambda_g$, 1 for $\lambda > \lambda_g$.

Unfortunately, because of the effect of direction on optical lengths and hence on the level of interference, the transmission and reflection coefficients depend strongly upon the angle of incidence. For black-body radiation the dependence of the normal component of power upon
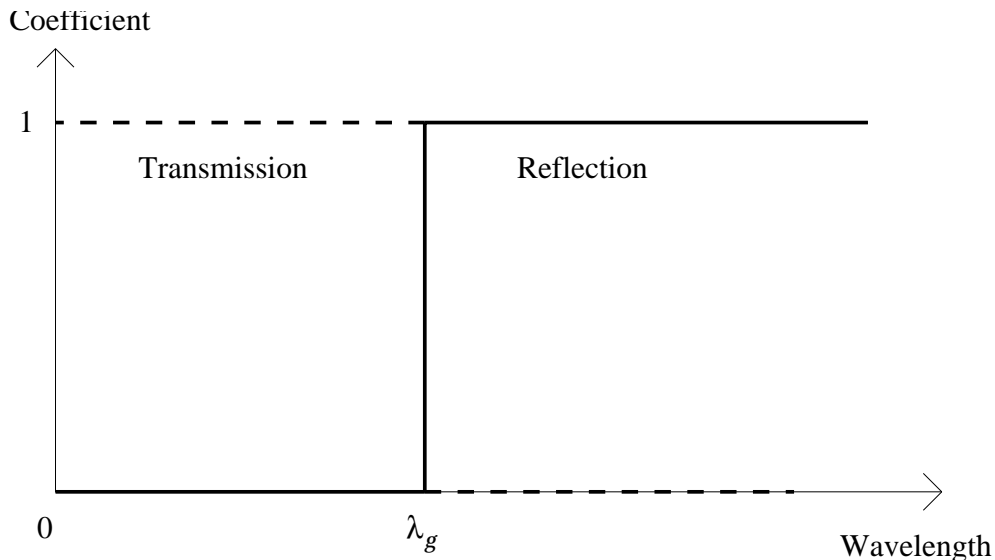
Figure 1: Ideal reflection and transmission coefficients as functions of wavelength λ.

the angle of incidence α exhibits a maximum at $\alpha = \pi/4$, although, of course, the power density (with respect to angle) is positive for all $0 < \alpha < \pi/2$. This means that – assuming that black-body radiation is impinging on the TPV cell – it makes sense to try to optimize the filter's performance for $\alpha = \pi/4$, but then most radiation will be incident along sub-optimal directions. Indeed, because the optical lengths inside the filter are essentially given by $\cos \alpha$ (or $\sec \alpha$), the effectivenesss of the filter depends least strongly upon angle for α near 0 (normal incidence). For this reason attention must also be focused on trying to direct the light from the radiator (Sections 3 and 4). With light travelling in (roughly) one direction, it is then possible to orient the cells so that light falls on them normally and the interference filters should be designed to work optimally with $\alpha = 0$ (or small).

A second design improvement is also worthy of mention. It was raised during our deliberations, but constraints on time prevented us from further examining this research topic. The black-body radiation spectrum is not immutable; it is modified by using a multiple dielectric layer design for the emitter. This has the advantage of controlling both the angular emission pattern and the emission spectrum. This concept is briefly discussed at the end of Section 2.

2   The Interference Filter

The filter consists of a large number of thin layers of differing optical properties. Two approaches might be used in seeing how light is transmitted and reflected by the layers. The first could involve looking for harmonic solutions, $\boldsymbol{E} = \mathrm{Re}\{\tilde{\boldsymbol{E}}e^{i\omega t}\}$, for the electric field in a heterogeneous medium. For electrical permittivity ϵ and magnetic permeability μ depending

2

on the spatial coordinate z perpendicular to the cell, $\boldsymbol{E}$ satisfies

$$\epsilon\mu\frac{\partial^2\boldsymbol{E}}{\partial t^2} = \nabla^2\boldsymbol{E} + \frac{1}{\mu}\frac{d\mu}{dz}\boldsymbol{k}\times(\nabla\times\boldsymbol{E}) + \nabla\left(\boldsymbol{E}\!\cdot\!\boldsymbol{k}\frac{d\epsilon}{dz}\right) ,$$

where $\boldsymbol{k}$ is the unit vector in the z direction. ($c = 1/\sqrt{\epsilon\mu}$ is the local speed of light.) Writing $\boldsymbol{E} = (E_1, E_2, E_3)$, the last two terms are

$$\frac{1}{\mu}\frac{d\mu}{dz}\left(\frac{\partial E_3}{\partial x} - \frac{\partial E_1}{\partial z}, \frac{\partial E_3}{\partial y} - \frac{\partial E_2}{\partial z}, 0\right) + E_3\frac{d^2\epsilon}{dz^2}\boldsymbol{k} + \frac{d\epsilon}{dz}\nabla E_3 .$$

Now writing $\boldsymbol{E} = \mathrm{Re}\{\tilde{\boldsymbol{E}}e^{i\omega t}\}$, $\boldsymbol{E}$ is given, in principle, by solving the following equation for $\tilde{\boldsymbol{E}}$:

$$\nabla^2\tilde{\boldsymbol{E}} + \omega^2\epsilon\mu\tilde{\boldsymbol{E}}\frac{1}{\mu}\frac{d\mu}{dz}\boldsymbol{k}\times(\nabla\times\tilde{\boldsymbol{E}}) + \tilde{E}_3\frac{d^2\epsilon}{dz^2}\boldsymbol{k} + \frac{d\epsilon}{dz}\nabla\tilde{E}_3 = 0 ,$$

with appropriate boundary conditions. Although this approach can cope with quite general continuous heterogeneous media, it was not taken further. Instead more attention was directed towards the second.

In any one layer, permittivity ϵ and permeability μ are both constant. Maxwell's equations (for zero electric current and vanishing charge density),

$$\frac{\partial\boldsymbol{D}}{\partial t} = \nabla\times\boldsymbol{H} , \quad \frac{\partial\boldsymbol{B}}{\partial t} = -\nabla\times\boldsymbol{E} , \quad \nabla\!\cdot\!\boldsymbol{B} = \nabla\!\cdot\!\boldsymbol{D} = 0 ,$$

with

$$\boldsymbol{B} = \mu\boldsymbol{H} , \quad \boldsymbol{D} = \epsilon\boldsymbol{E} ,$$

lead to the vector wave equation

$$\frac{\partial^2\boldsymbol{E}}{\partial t^2} = c^2\nabla^2\boldsymbol{E} ,$$

where again $c^2 = 1/\epsilon\mu$.

For an electromagnetic filed associated with a light ray travelling in the x-z plane and making an angle α (also called the angle of incidence) with the z axis, $\boldsymbol{E}$ is a sinusoidal plane wave,

$$\boldsymbol{E} = \mathrm{Re}\left\{\tilde{\boldsymbol{E}}e^{ik(ct-z\cos\alpha-x\sin\alpha)}\right\} ,$$

where k is now the wave number and $(\sin\alpha, 0, \cos\alpha)$ is the unit vector in the direction of the ray.

The ray can given in terms of plane-polarized light:

(I): $\boldsymbol{E}$ in the y direction so $\tilde{\boldsymbol{E}} = (0, A, 0)$ and, correspondingly, $\tilde{\boldsymbol{B}} = \dfrac{A}{c}(-\cos\alpha, 0, \sin\alpha)$ ($\boldsymbol{B} = \mathrm{Re}\left\{\tilde{\boldsymbol{B}}e^{ik(ct-z\cos\alpha-x\sin\alpha)}\right\}$).
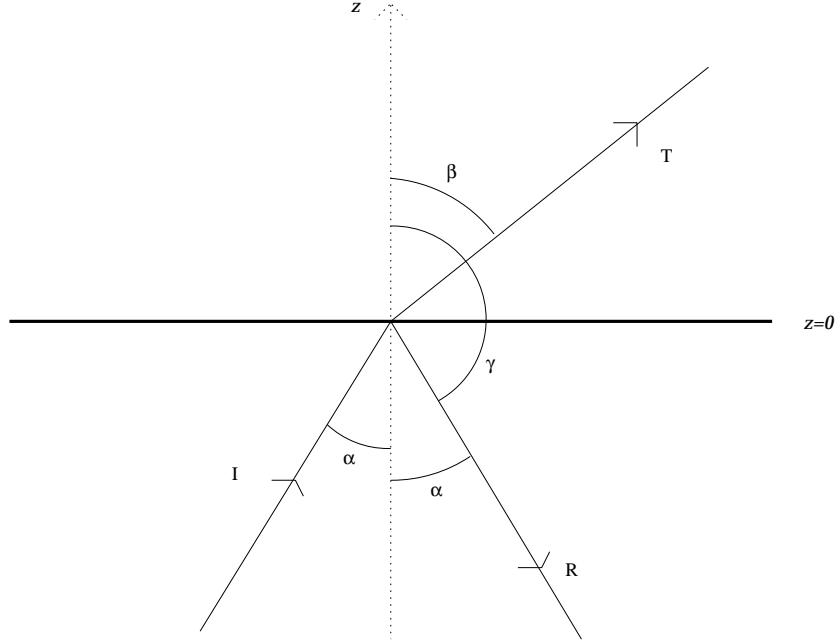
3

Figure 2: Light reflected and transmitted at the interface $z = 0$.

(II): $\boldsymbol{E}$ lying in the x–z plane so $\tilde{\boldsymbol{E}} = A(\cos\alpha, 0, -\sin\alpha)$ and $\tilde{\boldsymbol{B}} = \dfrac{A}{c}(0, 1, 0)$.

In each case A is the complex amplitude of the electric field and contains information about the phase as well as the magnitude.

At an interface, say $z = 0$ for the present, between two media with permittivities ϵ_a, ϵ_b and permeabilities μ_a, μ_b lying in $z < 0$, $z > 0$ respectively, an incoming wave

$$\tilde{\boldsymbol{E}}_I e^{ik(ct - z\cos\alpha - x\sin\alpha)}$$

in $z < 0$ undergoes reflection and refraction so there are a reflected plane wave

$$\tilde{\boldsymbol{E}}_R e^{ik(ct - z\cos\gamma - x\sin\gamma)}$$

and a transmitted one

$$\tilde{\boldsymbol{E}}_T e^{ik(ct - z\cos\beta - x\sin\beta)} \ ;$$

$\gamma = \pi - \alpha$. (See Fig. 2.)

At the interface the tangential components of $\boldsymbol{E}$ and of $\boldsymbol{H}$ and the normal components of $\boldsymbol{B}$ and $\boldsymbol{D}$ are continuous:

$$E_{a1} = E_{b1} , \quad E_{a2} = E_{b2} , \quad \epsilon_a E_{a3} = \epsilon_b E_{b3} ,$$

$$B_{a1}/\mu_a = B_{b1}/\mu_b , \quad B_{a2}/\mu_a = B_{b2}/\mu_b , \quad B_{a3} = B_{b3} .$$

4

Applying these six conditions to the total field in $z < 0$,

$$\tilde{\boldsymbol{E}}_I e^{ik(ct - z\cos\alpha - x\sin\alpha)} + \tilde{\boldsymbol{E}}_R e^{ik(ct + z\cos\alpha - x\sin\alpha)} \ ,$$

and the transmitted field in $z > 0$ gives, for both polarisations, $\sin\beta/\sin\alpha = \sqrt{\epsilon_a \mu_a / \epsilon_b \mu_b} = c_b/c_a$ (Snell's law) and:

(I)

$$\frac{A_R}{A_I} = \frac{\sqrt{\epsilon_a/\mu_a}\cos\alpha - \sqrt{\epsilon_b/\mu_b}\cos\beta}{\sqrt{\epsilon_a/\mu_a}\cos\alpha + \sqrt{\epsilon_b/\mu_b}\cos\beta} \tag{1}$$

and

$$\frac{A_T}{A_I} = \frac{2\sqrt{\epsilon_a/\mu_a}\cos\alpha}{\sqrt{\epsilon_a/\mu_a}\cos\alpha + \sqrt{\epsilon_b/\mu_b}\cos\beta} \ ; \tag{2}$$

(II)

$$\frac{A_R}{A_I} = \frac{\sqrt{\mu_a/\epsilon_a}\cos\alpha - \sqrt{\mu_b/\epsilon_b}\cos\beta}{\sqrt{\mu_a/\epsilon_a}\cos\alpha + \sqrt{\mu_b/\epsilon_b}\cos\beta}$$

and

$$\frac{A_T}{A_I} = \frac{2\sqrt{\mu_b/\epsilon_b}\cos\alpha}{\sqrt{\mu_a/\epsilon_a}\cos\alpha + \sqrt{\mu_b/\epsilon_b}\cos\beta} \ .$$

It has been assumed here that total internal reflection does not occur ($|\sin\alpha| < c_b/c_a$). (Taking zero angle of incidence, $\alpha = 0$, appears to give a discrepancy in the sign of the complex amplitude of the reflected wave in cases (I) and (II). This is simply due to the ways in which the fields have been written for the two polarisations.)

In the interference filter, this process of reflection and refraction happens at each internal boundary, see Fig. 3. Because $z \neq 0$ at the interfaces, extra care must be taken with phases.

The transmission and reflection relations can be used to determine equations for the complex amplitudes of the waves in the positive and negative z directions in layer m (A_m and C_m respectively). At the boundary $z = z_m$ between layers $m - 1$ and m, $m = 1, \ldots, M$ ($z < z_1$ is the exterior of the filter), using polarisation (I):

$$C_{m-1} e^{ikz_m \cos\alpha_{m-1}} = \frac{\sqrt{\epsilon_{m-1}/\mu_{m-1}}\cos\alpha_{m-1} - \sqrt{\epsilon_m/\mu_m}\cos\alpha_m}{\sqrt{\epsilon_{m-1}/\mu_{m-1}}\cos\alpha_{m-1} + \sqrt{\epsilon_m/\mu_m}\cos\alpha_m} A_{m-1} e^{-ikz_m \cos\alpha_{m-1}}$$

$$+ \frac{2\sqrt{\epsilon_m/\mu_m}\cos\alpha_m}{\sqrt{\epsilon_{m-1}/\mu_{m-1}}\cos\alpha_{m-1} + \sqrt{\epsilon_m/\mu_m}\cos\alpha_m} C_m e^{ikz_m \cos\alpha_m}$$
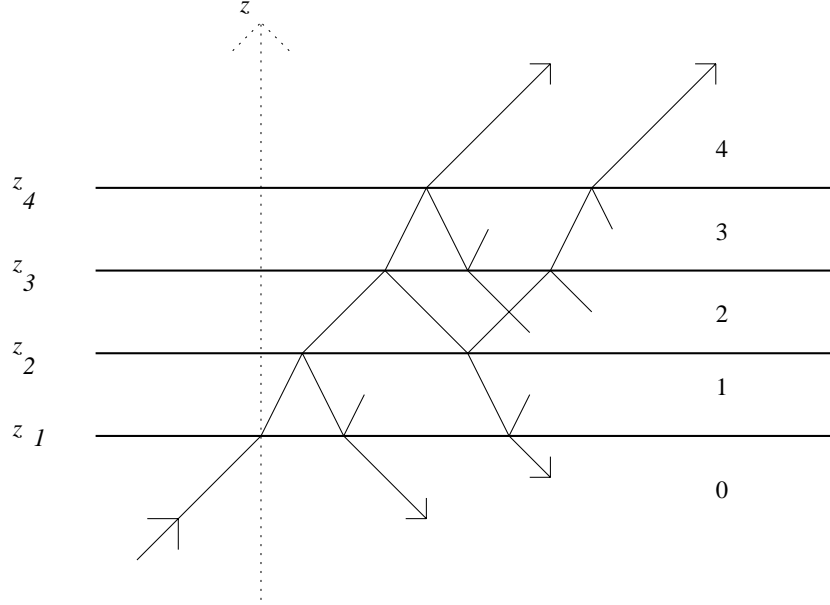
Figure 3: Multiple reflections and refractions for light moving between layers 0 (outside the filter), 1, 2, ….

(see (1) and (2)); and

$$A_m e^{-ikz_m \cos \alpha_m} = \frac{2\sqrt{\epsilon_{m-1}/\mu_{m-1}} \cos \alpha_{m-1}}{\sqrt{\epsilon_{m-1}/\mu_{m-1}} \cos \alpha_{m-1} + \sqrt{\epsilon_m/\mu_m} \cos \alpha_m} A_{m-1} e^{-ikz_m \cos \alpha_{m-1}}$$

$$+ \frac{\sqrt{\epsilon_m/\mu_m} \cos \alpha_m - \sqrt{\epsilon_{m-1}/\mu_{m-1}} \cos \alpha_{m-1}}{\sqrt{\epsilon_{m-1}/\mu_{m-1}} \cos \alpha_{m-1} + \sqrt{\epsilon_m/\mu_m} \cos \alpha_m} C_m e^{ikz_m \cos \alpha_m} \ .$$

Here the extra terms on the right-hand sides are due to the incoming wave moving down from $z > z_m$. The factors $e^{ikz_m \cos \alpha_{m-1}}$ *etc.* account for the non-zero value of z at the interface.

There are now $2M$ equations for $A_1, \ldots, A_M, C_0, \ldots, C_{M-1}$, given A_0, the incoming wave, and assuming that $C_M = 0$, *i.e.* that no light is returned from the TPV cell (or C_M is otherwise specified). The other polarisation can be handled similarly. (It is clear that, because of the different transmission and reflection coefficients for the two polarisations when $\alpha \neq 0$, light not arriving normally complicates matters.) The optimization procedure now entails making C_0/A_0 small for $k < k_g$ ($\lambda > \lambda_g$) and close to 1 for $k > k_g$, the useful radiation.

These equations are solved by matrix methods. The following MATLAB program was used to illustrate the results. A compact interference filter can be designed using the transfer matrix program. Most parameters are annotated in the main program. An interpolation function is used for dispersive dielectric properties, but this feature will not be demonstrated here. We note that the program has been tested using metal layers, an extreme case of the complex dielectric, where the imaginary contribution to the index exceeds the real one in magnitude.

6

```matlab
% Transfer matrix Program
%Calculate the transmission spectrum through a multiple thin film sample
%Written by Feiran Huang on 05/31/99. Last Update by Joe Haus 06/10/99
%-----------------------
%given: physical parameters for the films, n,k,and d for various wavelengths
% Vector of parameters
v=[300 2500 0 2];
% Angle of incidence
fi0=pi/4;
%film information
% Thickness of dielectric 1
d1=1500/4/3.5;
% Thickness of dielectric 2
d2=1500/4/1.5;
% Number of layers
m=5;
% range of wavelengths
lambda=v(1):1:v(2);
% Dispersive index of the superstrate
% Wavelengths
ld00=[180  3000];
% real part
n00=[1. 1.];
% complex index of dielectric 1
% Wavelengths
ld10=[180 3000];
% real part
n10=[3.5 3.5];
% imaginary part
k10=[0 0];
% complex index of dielectric 2
% Wavelengths
ld20=[180 3000];
% real part
n20=[1.5 1.5];
% imaginary part
k20=[0 0];
% dispersive index of the substrate
% wavelengths
ld30=[180 3000];
% real part
n30=[1. 1.];
```

```
% Interpolate the (in general) complex refractive indices for all wavelengths
% Index of the superstrate
n0=interp1(ld00,n00,lambda);
% complex index of dielectric 1
n1=interp1(ld10,n10,lambda);
k1=interp1(ld10,k10,lambda);
% Complex index of dielectric 2
n2=interp1(ld20,n20,lambda);
k2=interp1(ld20,k20,lambda);
% Index of the substrate
n3=interp1(ld30,n30,lambda);
%generate the p- and s-polarizations
[Tp,Rp,Ts,Rs]=f_2mlyr(n0,n1,k1,n2,k2,n3,d1,d2,m,fi0,lambda);

% Plot the results
figure(1);
hold on;
%plot(lambda, Tp,'k-');
plot(lambda, Tp,'k:');
ylabel('T_p ');
xlabel('Wavelength (nm)');
grid on;
axis(v);
figure(2);
hold on;
%plot(lambda, Ts,'k-');
plot(lambda, Ts,'k:');
ylabel('T_s ');
xlabel('Wavelength (nm)');
grid on;
axis(v);

% Function subroutine f_2lymr - multiply the transfer matrices
function [Tp,Rp,Ts,Rs]=f_2mlyr(n0,n1,k1,n2,k2,n3,d1,d2,m,fi0,lambda)
%calculate transmittance and reflectance of a multi-layer system
%Written by Feiran Huang 05/31/99.
% Last Updated and corrected 06/20/99 by Joe Haus
%------------------------
%
for n=1:length(lambda)
% Complex angles
   fi1=asin(sin(fi0)*n0(n)/(n1(n)+i*k1(n)));
```

```
    fi2=asin(sin(fi0)*n0(n)/(n2(n)+i*k2(n)));
    fi3=asin(sin(fi0)*n0(n)/n3(n));
    [r01p,t01p,r01s,t01s]=f_rtamp(n0(n),0,n1(n),k1(n),fi0,fi1);
    [r12p,t12p,r12s,t12s]=f_rtamp(n1(n),k1(n),n2(n),k2(n),fi1,fi2);
    [r21p,t21p,r21s,t21s]=f_rtamp(n2(n),k2(n),n1(n),k1(n),fi2,fi1);
    [r23p,t23p,r23s,t23s]=f_rtamp(n2(n),k2(n),n3(n),0,fi2,fi3);
    delta01=0;
    delta12=2*pi*(n1(n)-i*k1(n))*d1*cos(fi1)/lambda(n);
    delta21=2*pi*(n2(n)-i*k2(n))*d2*cos(fi2)/lambda(n);
    delta23=2*pi*(n2(n)-i*k2(n))*d2*cos(fi2)/lambda(n);
    C01p=[1 r01p; r01p 1];
    C12p=[exp(i*delta12) r12p*exp(i*delta12); r12p*exp(-i*delta12) exp(-i*delta12)];
    C21p=[exp(i*delta21) r21p*exp(i*delta21); r21p*exp(-i*delta21) exp(-i*delta21)];
    C23p=[exp(i*delta23) r23p*exp(i*delta23); r23p*exp(-i*delta23) exp(-i*delta23)];
    Ap=C01p*C12p;
    tp=t01p*t12p;
    for j=1:m-1
        Ap=Ap*C21p*C12p;
        tp=tp*t21p*t12p;
    end
    Ap=Ap*C23p;
    tp=tp*t23p;
    Rp(n)=abs(Ap(2,1)/Ap(1,1))^2;
    Tp(n)=n3(n)*cos(fi3)/n0(n)/cos(fi0)*abs(tp/Ap(1,1))^2;
    C01s=[1 r01s; r01s 1];
    C12s=[exp(i*delta12) r12s*exp(i*delta12); r12s*exp(-i*delta12) exp(-i*delta12)];
    C21s=[exp(i*delta21) r21s*exp(i*delta21); r21s*exp(-i*delta21) exp(-i*delta21)];
    C23s=[exp(i*delta23) r23s*exp(i*delta23); r23s*exp(-i*delta23) exp(-i*delta23)];
    As=C01s*C12s;
    ts=t01s*t12s;
    for j=1:m-1
        As=As*C21s*C12s;
        ts=ts*t21s*t12s;
    end
    As=As*C23s;
    ts=ts*t23s;
    Rs(n)=abs(As(2,1)/As(1,1))^2;
    Ts(n)=n3(n)*cos(fi3)/n0(n)/cos(fi0)*abs(ts/As(1,1))^2;
end

% function subroutine f_rtamp
function [rp,tp,rs,ts]=f_rtamp(n1,k1,n2,k2,fi1,fi2)
```

```
%calculate the complex transmission and reflection amplitude
%Written by Feiran Huang on 05/31/99. Last Update 05/31/99
%------------------------
%given index and absorption
n1=n1-i*k1;
n2=n2-i*k2;
rp=(n1*cos(fi2)-n2*cos(fi1))/(n1*cos(fi2)+n2*cos(fi1));
rs=(n1*cos(fi1)-n2*cos(fi2))/(n1*cos(fi1)+n2*cos(fi2));
tp=2*n1*cos(fi1)/(n1*cos(fi2)+n2*cos(fi1));
ts=2*n1*cos(fi1)/(n1*cos(fi1)+n2*cos(fi2));
```

Two figures are generated from the transfer matrix program. For simplicity the layers are a quarter-wavelength thick with the center wavelength given as 1.5 μm. The refractive indices are $n_1 = 3.5$ and $n_2 = 1.5$; the first is typical of a semiconductor material, while the second is typical of a wide electronic bandgap insulator. No attempt was made here to put in real physical parameters; the program has the capability to enter complex index parameters and to interpolate from a set of values. The superstrate and substrate materials are assumed to be vacuum. Using these parameters and 5 periods of dielectric a large transmission stop band covering the wavelength range from 1.1 μm to about 2 μm. This filter is less than 2 μm thick, very compact indeed.

Two polarizations are distinguished in the analysis. The P-polarized wave has its electric field vector in the plane of incidence, i.e. the plane defined by the incident, reflected and transmitted wave vectors, and the S-polarization has it confined perpendicular to the plane of incidence. The two polarizations are indistinguishable at normal incidence ($\alpha = 0$).

The larger issue is the dependence of the transmission on the angle of incidence of the radiation. Large variations will spoil the figure of merit of the filter. In Fig. 4 the p-polarization transmission function is shown for two angles of incident $\alpha = 0, \pi/4$. The edges of the stop bands shift by about 10 percent over this range. For larger angles the shift becomes even larger. The S-polarization has a similar angular dependence with a 10 percent shift of the band edge near 1.1 μm. Both have a larger shift of the gap near 500 nm.

Evaluation of the angular dependence highlights a problem for the operation of the interference filters: the efficiency of the filter cannot be designed for optimal performance at all wavelengths, unless some new concept is introduced. This problem is relevant because blackbody radiation is distributed over all angles with a maximum irradiance occurring at $\alpha = \pi/4$. However, for a range of say $30°$ about this point, the variations in the transmission curves are much larger.

Two potential solutions to this problem are considered: 1.) change the angular distribution of the radiation; and 2.) alter the spectral emission of the black-body radiator. The former is considered in the next section. The latter problem has a solution akin to the interference filter, i.e. design the radiator with a periodic set of absorbing layers so that the emission at undesirable wavelengths are suppressed and emission at desired wavelengths is enhanced. A simple model for engineering the black-body radiation pattern was used by Cornelius and Dowling [1]. The off-axis work in their paper is of limited use, as it treats only cases with real
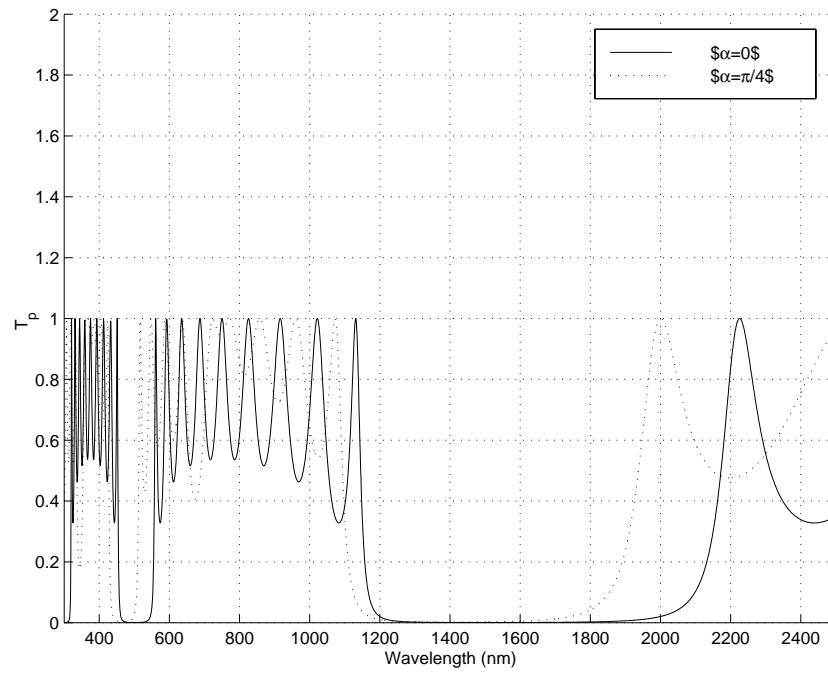
Figure 4: P-polarization transmission for two angle of incidence $\alpha = 0$ and $\alpha = \pi/4$. Parameters are given in the text.
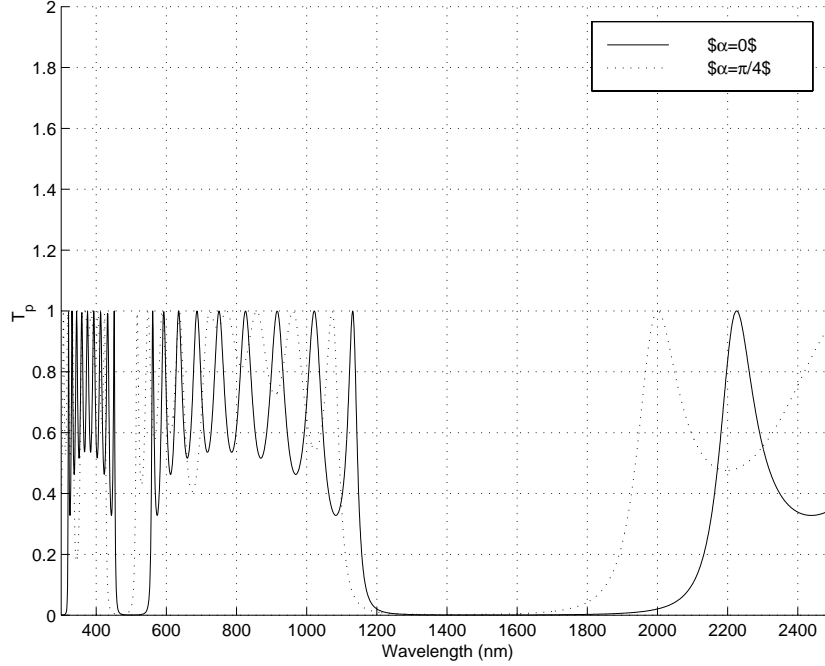
Figure 5: S-polarization transmission for two angle of incidence $\alpha = 0$ and $\alpha = \pi/4$.

dielectric constants. However, for zero angle of incidence they displayed the desired effects. The emission was suppressed in regions with a band gap and enhanced emission was found at the band edges.

3 Directionality of the Radiation

The characteristics of black-body radiation coming from different directions should perhaps be first stated clearly. For any particular wavelength, light originating on a black body is evenly distributed, according to **solid angle**, over all directions. Taking spherical polar coordinates (r, φ, θ) with $\theta = 0$ (the z axis) directed perpendicularly out of the black body (or normally into a TPV cell), the uniform energy density with respect to solid angle becomes $\sin\theta$: the energy $d\Omega$ ($d\tilde{\boldsymbol{E}}$?) at some point and in the solid angle $d\Omega$ is $\sin\theta \, d\theta \, d\varphi$ in terms of polars. (A scaling of the black-body energy is assumed to make the density, with respect to solid angle, unity. Equivalently, for the wavelength being considered, the total energy density at a point in a cavity enclosed by a black body, at the temperature of interest, is 4π; this is reduced to 2π for energy coming from a plane, with energy radiating off to infinity.) For this application, it is power, rather than energy, which is of interest. The normal component of the energy flux $\boldsymbol{q}$ (power density) is then multiplied by $\boldsymbol{n} \cdot \boldsymbol{q}/|\boldsymbol{q}| = \cos\theta$:

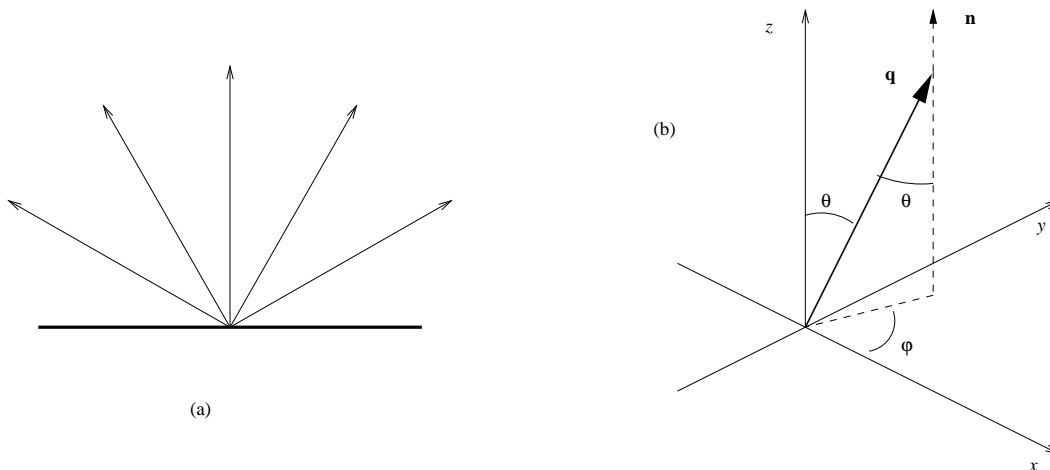$$\text{power entering the cell per unit area} \; = \sin\theta \cos\theta \, d\theta \, d\varphi \; .$$

Figure 6: (a) Uniform black-body radiation. (b) Polar coordinates.

The dependence upon the angle of incidence, θ, only, is given by integrating over φ to obtain $\pi \sin 2\theta \, d\theta$ and it is this power density $\pi \sin 2\theta$ which achieves its maximum at $\theta = \pi/4$.

An important aspect of the problem is then the question: can the radiation be directed (so that the energy density is concentrated near $\theta = 0$ on orienting the TPV cell appropriately)?

One simple way of doing this is to have a very small radiator, a point source, and arranging cells over the surface of a sphere centred on the source. This has a couple of drawbacks, one of which is that there is only a small source of energy (which also has to be supported inside the sphere). Another difficulty, which will recur, is that the "bad" radiation will not, in general, be reflected exactly back to the radiator. This will lead to more generally directed low-frequency radiation inside the cavity (of black-body type unless a significant proportion can escape to or through the sphere).

Variations of this might be:

  (i) to use a line source, or a thin cylindrical radiator, inside a larger concentric cylinder of cells, to obtain a bigger radiating surface (and avoid any difficulties in supporting it);

 (ii) employ a paraboloidal reflector to get parallel rays normal to a plane array of cells, which no longer has to enclose the point source;

(iii) combine these, with a line source along the focus of a parabolic cylindrical reflector.

All of these still have a source of small surface area, while (i) and (iii) will also give rise to less directed radiation (with a component parallel as well as normal to the line source).

Another idea thought of briefly was to try to direct the light rays by placing some transparent object, say a wedge of glass, in front of the cells (Fig. 7).
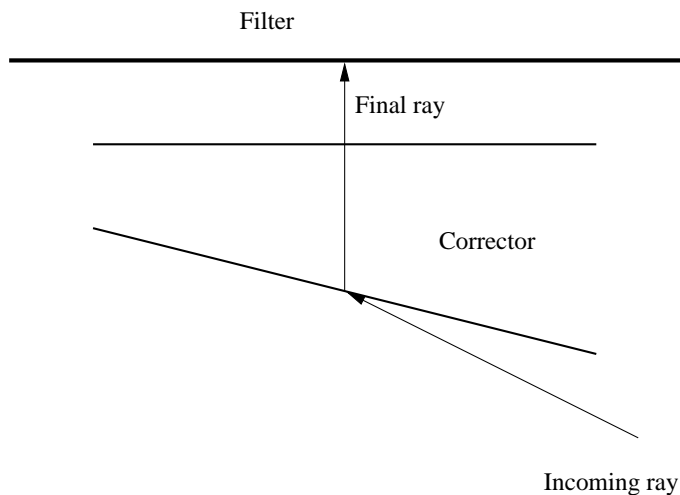
13

Figure 7: A correcting wedge below the filter.

This was seen to fail because to get small variation of the direction of the transmitted light, the incoming ray would have to be nearly parallel to the lower surface of the glass, as shown in Fig. 7, and also because the light is actually travelling in three dimensions, not necessarily in the plane of this figure.

This leaves the possibility of varying the actual surface of the radiator.

4   Effect of Non-Uniform Radiator Surface

The simplest idea was to try instead of a flat black surface, a grooved or dimpled black surface. This can be quickly rejected because of the nature of black-body radiation: the energy density at a point is simply the solid angle subtended at that point by the emitting surface. (Equivalently, for any direction passing through the point from the radiator surface, the energy density per unit solid angle is 1. See Fig. 8.)

What might help, however, is to have a curved surface with some emitting (black) parts and some reflecting parts. Such a two-dimensional arrangement is sketched in Fig. 9, and has pits or indentations in the surface, each with a black bottom and reflecting sides.

This idea has previously been considered in the literature, [2], [3]. Taking the surface to be covered by a large number of such small, three-dimensional pits, it is clear that they should be relatively narrow and deep, to restrict the angle of emission (but they should not be parallel-sided since, if they were, a light ray would keep the same angle to the overall normal, the z axis, as it bounced up the pit). They should also be black at or near the bottom.

Taking a typical top radius (radius of the opening of the pit) to be b, bottom radius (where the black part ends) to be a, and depth (normal distance from the opening to the black part) to be h (Fig. 10), then:
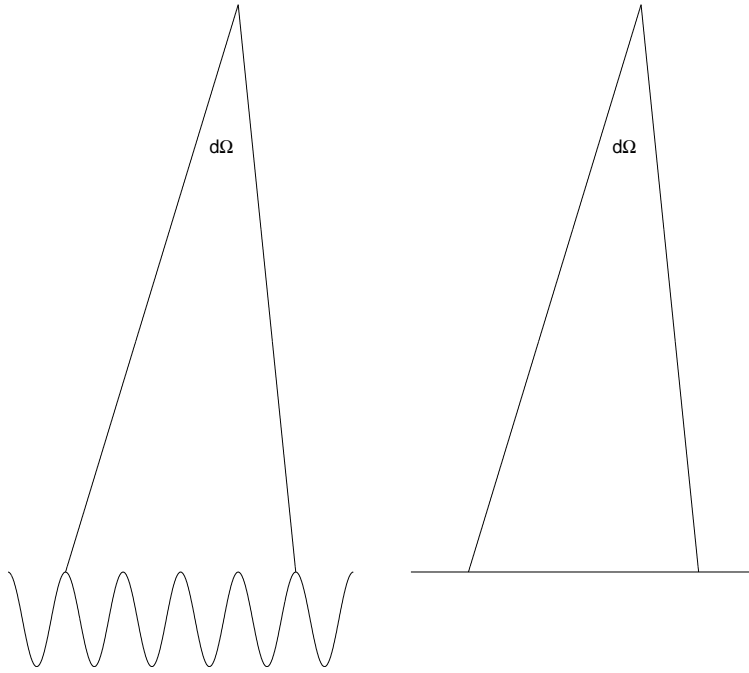
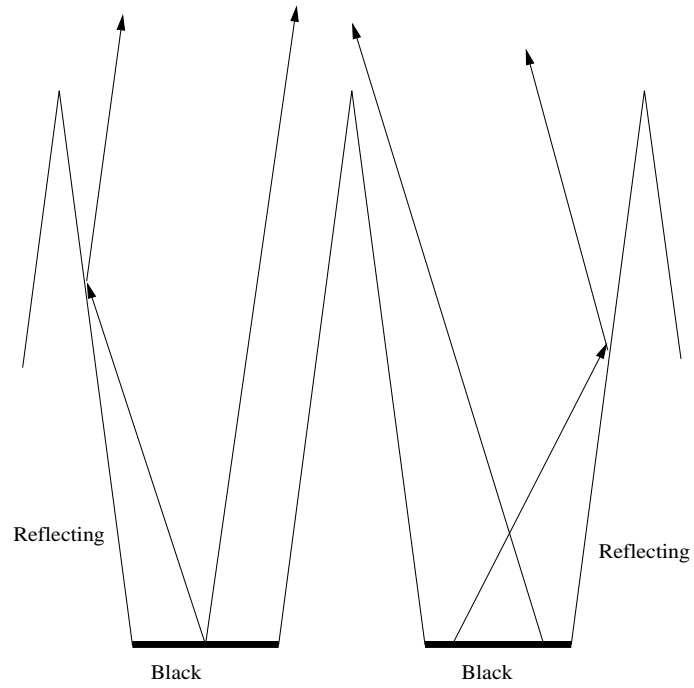Figure 8: Identical energy densities from different surfaces.
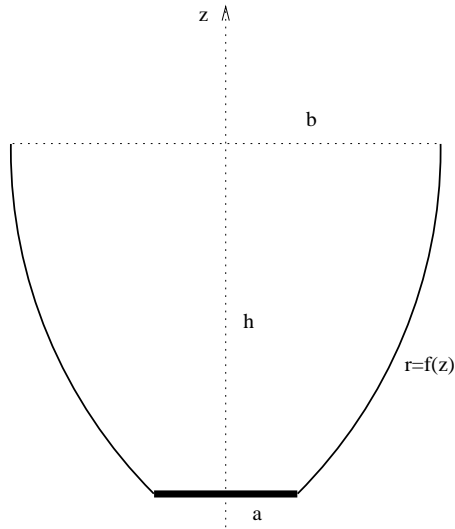

Figure 9: Light-emitting grooves.

Figure 10: A light-emitting pit.

- to restrict the direction of emission, $b \ll h$;

- to avoid diffraction, $b \gg \lambda$;

- to get reflection to limit the angle of emission, $a < b$;

- to have a reasonable light-emitting proportion of the surface area, $a \not\ll b$.

Three ways of determining the normal component of the power density emitted by such a surface were discussed.

4.1 Ray tracing with a Monte-Carlo simulation.

Since the black-body power distribution is known – uniform as a function of position on the bottom surface and azimuthal angle φ but with directional dependence $\sin\theta$ on emission angle θ – it is possible to carry out a Monte-Carlo simulation with light being emitted randomly from the flat bottom surface. (The positional and directional distribution of rays, or photons, is the power distribution.) The resulting rays are traced, following each reflection as they hit the side surface, to determine the final angle leaving the pit. A power distribution as a function of the ultimate θ (which would be the incident angle on a flat surface such as a TPV cell parallel to the overall radiationg surface) then results.

Three sets of simulations were done for pits as shown in Fig. 11:

- Two dimensions with trapezoidal holes, the trapezia having parallel sides $2a$ and $2b$, width h, and sides angled at α to the normal.
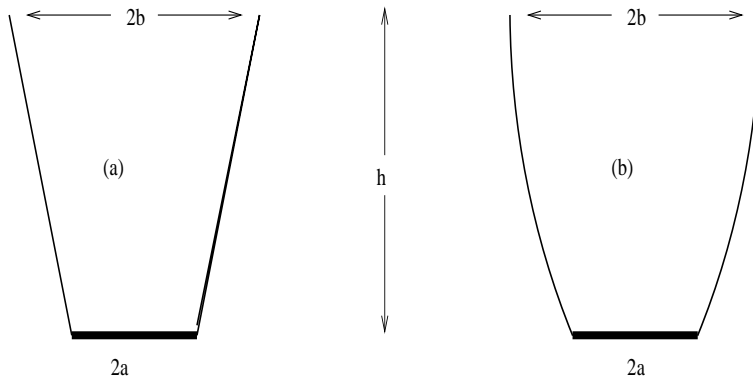
Figure 11: Shapes used in Monte-Carlo simulations. (a) Two dimensions and a frustum in three dimensions. (b) A paraboloid.

- Three dimensions, conical frusta, with bottom radii a, top radii b, and sides with angles α.

- Three dimensions, with paraboloidal pits, of various aspect ratios.

Some results are shown at the end of this report.

4.2 Particular high-aspect-ratio asymptotics.

Following [4], one special case where progress can be made, and which does not require that the light wavelength be much smaller than any simple combination of geometrical length scales, is when
$$\frac{\lambda}{R} \sim \frac{R}{h} \ll 1$$
(λ is again wavelength and R is a typical hole radius, or dimension across the pit). For light of wavelength $10\,\mu$m, this could allow pits of depth 1 mm and width 0.03 mm.

Scaling the normal distance with respect to h and radius with $R \sim \sqrt{\lambda h}$, and now writing $\boldsymbol{E} = \mathrm{Re}\{\tilde{\boldsymbol{E}}(\boldsymbol{x})e^{i\omega t}\}$, the Helmholtz equation satisfied by any component of $\tilde{\boldsymbol{E}}$ (or of $\tilde{\boldsymbol{B}}$) within a pit of circular cross-section is changed from
$$\frac{\partial^2 u}{\partial z^2} + \frac{\partial^2 u}{\partial r^2} + \frac{1}{r}\frac{\partial u}{\partial r} + k^2 u = 0,$$
where k is the wave number, to
$$\frac{\partial^2 u}{\partial Z^2} + K\left(\frac{\partial^2 u}{\partial \rho^2} + \frac{1}{\rho}\frac{\partial u}{\partial \rho}\right) + K^2 u = 0 \ ,$$
where $K = kh \gg 1$ is a dimensionless wave number, Z is z scaled, and ρ is r scaled. Looking for a solution in the form
$$u = e^{iKZ}U \ , \tag{3}$$

17

to leading order U satisfies the Schrödinger equation

$$2i\frac{\partial U}{\partial Z} + \frac{\partial^2 U}{\partial \rho^2} + \frac{1}{\rho}\frac{\partial U}{\partial \rho} = 0 \ . \tag{4}$$

To find how the field varies outside the pit, the same *ansatz* (3) and equation (4) are taken to hold. Looking at relatively large distances, further scaling is necessary. By writing $Z = \xi/\delta$ and $\rho = \eta/\delta$, with $\delta \ll 1$, (4) becomes

$$2i\frac{\partial U}{\partial \xi} + \delta\left(\frac{\partial^2 U}{\partial \eta^2} + \frac{1}{\eta}\frac{\partial U}{\partial \eta}\right) = 0$$

and trying

$$U \sim \Phi e^{\Psi/\delta}$$

gives

$$\frac{2i}{\delta}\Phi\frac{\partial \Psi}{\partial \xi} + 2i\frac{\partial \Phi}{\partial \xi} + \frac{\Phi}{\delta}\left(\frac{\partial \Psi}{\partial \eta}\right)^2 + 2\frac{\partial \Phi}{\partial \eta}\frac{\partial \Psi}{\partial \eta} + \Phi\frac{\partial^2 \Psi}{\partial \eta^2} + \frac{1}{\eta}\Phi\frac{\partial \Psi}{\partial \eta} + \ldots = 0 \ .$$

A solution for Ψ, from $2i\dfrac{\partial \Psi}{\partial \xi} = \left(\dfrac{\partial \Psi}{\partial \eta}\right)^2$, is $\Psi = \dfrac{i\eta^2}{2\xi}$ and then

$$\xi\frac{\partial \Phi}{\partial \xi} + \eta\frac{\partial \Phi}{\partial \eta} + \Phi = 0$$

so

$$\Phi = \frac{1}{\xi}F\left(\frac{\eta}{\xi}\right) \ .$$

Then $u \sim \text{const.} Z^{-1}F(\rho/Z)e^{i(KZ+\delta\rho^2/2Z)}$ so that $|u|^2 \sim Z^{-2}F(\rho/Z)^2$: as well as the usual inverse square decay the presence of the $F(\rho/Z)$ term indicates that the wave is confined to a cone $\rho \lesssim CZ$, or $r \lesssim CRz/h$. Because of the smallness of the aspect ratio R/h, this indicates a narrow cone and a confined beam, $\theta \lesssim CR/h$. The value of C depends upon F and this in turn depends upon the solution of (4) subject to appropriate initial (bottom-of-the-pit) and boundary conditions. This still requires extra work because:

1. The boundary conditions should be reflecting and they really apply to the vector quantity $\tilde{\boldsymbol{E}}$, whose polarisation is affected by reflection at the boundary. A guide could be given by using the scalar equation and imposing either $\dfrac{\partial u}{\partial n} = 0$ or $u = 0$ on the boundary; neither can be expected to give a quantitatively correct answer.

2. The initial condition, due to a black-body source on $z = 0$, is not at all clear. One possibility might be to take $u = 1$ on $z = 0$. A better idea might be to solve a local problem, where $\zeta \equiv z/R = O(1)$, and then match with $Z = O(1)$. This still requires that some sort of point-source and radiation conditions be given on $z = \zeta = 0$. If a solution u is found which depends on some parameter ν, for example, the precise position of a source, the quantity of final interest might not be $u(\boldsymbol{x}, \nu)$ but instead some sort of average over all values of ν, *e.g.* $\int |u|\, d\nu$ or $\int |u|^2\, d\nu$, and possibly including some weight function. The latter integral might represent the total power of black-body radiation.
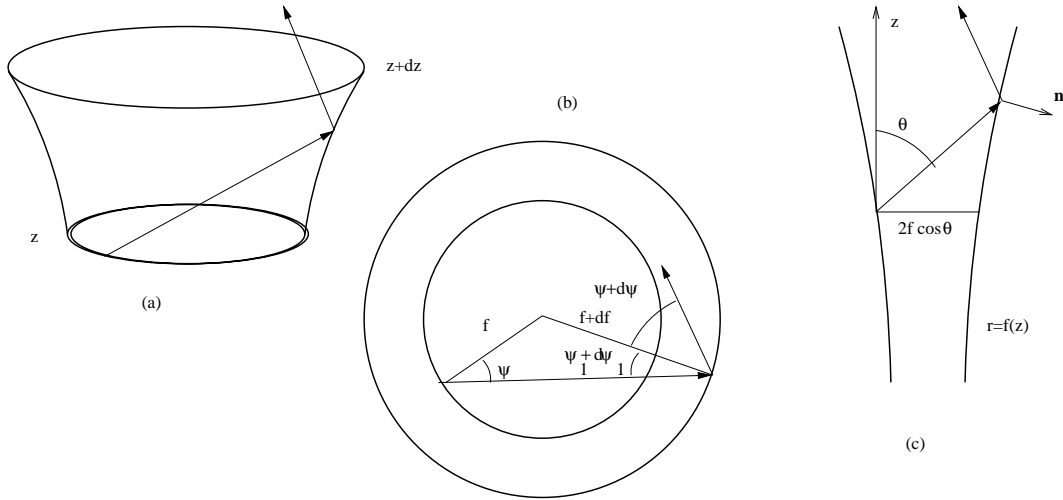
Figure 12: A ray being reflected up a pit (a) with its horizontal (b) and vertical (c) projections.

It has been assumed here that the *ansatz* (3) applies. This **might** result from the correct sort of boundary condition causing the pit to act as a wave guide and bringing about a plane-wave solution for u as ζ gets large.

4.3 Many reflections in a narrow pit.

Light emitted from the base of a long thin pit will be reflected many times as it travels up and out (unless the angle of emission θ is already small – but only a minute fraction of the power has $\theta \ll 1$). For convenience, a pit of circular cross-section is considered: it has base $z = 0$ (blackened), top $z = h$ (open) and curved surface $r = f(z)$ for $0 < z < h$ (reflecting). ($0 < a = f(0) < b = f(h) \ll h$.) The direction of a ray at any given point can be given in terms of the usual spherical polar angles θ and φ, with θ the angle between the ray and the z axis. Light rays can also be characterized by the direction at which they leave, and arrive at, the reflecting surface $r = f$: ψ will be a "horizontal angle of reflection". More precisely, it is the angle between the projections of the departing light ray and the inward normal, $-\boldsymbol{n}$, onto the x-y plane. See Fig. 12.

To leading order (in f/h), the distance travelled up the pit between successive reflections is

$$dz = 2f \cos \psi \cot \theta \ .$$

The outward normal $\boldsymbol{n}$, to leading order, is

$$\boldsymbol{n} = (-f', 1, 0) \ ,$$

using cylindrical polars (z, r, ϕ). In the same coordinates, the incident ray has direction

$$\boldsymbol{u} = (\cos \theta, \sin \theta \cos \psi_1, \sin \theta \sin \psi_1) \ ,$$

19

and the reflected ray has direction

$$\boldsymbol{v} = (\cos(\theta + d\theta), -\sin(\theta + d\theta)\cos(\psi_1 + d\psi_1), \sin(\theta + d\theta)\sin(\psi_1 + d\psi_1)) .$$

The "horizontal incident angle" ψ_1 will be related to the horizontal reflection angle ψ shortly; the new reflection angle is $\psi_1 + d\psi_1 \equiv \psi + d\psi$.

Since the angle of incidence is the same as the angle of reflection,

$$\boldsymbol{n}{\cdot}\boldsymbol{u} = -\boldsymbol{n}{\cdot}\boldsymbol{v}$$

so, to leading order,

$$-\cos\theta\cos\psi\, d\theta + \sin\theta\sin\psi\, d\psi_1 = 2f'\cos\theta . \tag{5}$$

Also the normal and two rays are coplanar so $(\boldsymbol{n}\times\boldsymbol{u}){\cdot}\boldsymbol{v} = 0$. After some manipulation, again to leading order, this gives

$$-\sin\psi\, d\theta - \cos\theta\sin\theta\cos\psi\, d\psi_1 = 2f'\sin^2\theta\cos\psi\sin\psi . \tag{6}$$

Solving (5), (6) leads to

$$d\theta = -2f'\cos\psi \qquad \text{and} \qquad d\psi_1 = 2f'\cot\theta\sin\psi .$$

Now relating ψ_1 to the earlier angle ψ,

$$\frac{\sin\psi_1}{f} = \frac{\sin\psi}{f + df}$$

so

$$f\sin\psi + (\psi_1 - \psi)f\cos\psi + \sin\psi\, df = f\sin\psi$$

and

$$\psi_1 - \psi = -\frac{f'\, dz}{f}\tan\psi = -2f'\sin\psi\cot\theta ,$$

to leading order. This means that

$$d\psi = \psi_1 + d\psi_1 - \psi = 0 .$$

Finally,

$$\frac{d\theta}{dz} = -\frac{f'}{f}\tan\theta \qquad \text{and} \qquad \frac{d\psi}{dz} = 0 ,$$

for any light ray as it travels up the pit.

Then

$$\psi = \text{ constant} \qquad \text{and} \qquad f(z)\sin\theta = \text{ constant.} \tag{7}$$

In particular, since at $z = 0$ (the bottom of the pit), $0 \le \sin\theta \le 1$, as the light exits from the top $(z = h)$,

$$0 \le \sin\theta \le f(0)/f(h) = a/b . \tag{8}$$

Hence the emission angle is no greater than $\sin^{-1}(a/b) \sim a/b$ for $a \ll b$. In terms of the fraction of the overall surface (say a convex surface stretched over the radiator) area which actually emits radiation,

$$\theta \lesssim C\sqrt{\text{area fraction}} \ .$$

(The constant C has to be introduced to account for the fact that the surface will not be entirely made up of the dimples. If it were, C would be 1.) The upper bound on angle θ, (8), shows good agreement those obtained with the Monte-Carlo simulations.

Equation (7) can be used to relate the ultimate angular power density to the intitial distribution $2\pi \sin \theta_0 \cos \theta_0$, where $0 < \theta_0 < \pi$ is the angle at the bottom of the pit. Integrating this density with respect to θ_0 and changing the variable of integration to the final angle θ (given by $b \sin \theta = a \sin \theta_0$) gives an emission power density

$$\frac{\pi b^2}{a^2} \sin 2\theta \text{ for } 0 < \theta < \sin^{-1}(a/b) \ , \quad 0 \text{ for } \sin^{-1}(a/b) < \theta \ .$$

To allow for imperfect reflection and a slight emission of radiation from the sides of such a hole, the transfer of energy in (z, θ, ψ) space can be examined. From the above calculations, following a photon,

$$\frac{dz}{dt} = c \cos \theta \ , \quad \frac{d\theta}{dt} = -2c\frac{f'}{f} \sin \theta \ , \quad \frac{d\psi}{dt} = 0 \ , \tag{9}$$

where c is again the speed of light. Then, for conservation of energy,

$$\frac{\partial}{\partial z}\left((c \cos \theta)E \right) + \frac{\partial}{\partial \theta}\left(\left(-2c\frac{f'}{f} \sin \theta \right) E \right) + \frac{\partial}{\partial \psi}(0E) = \text{net source}, \tag{10}$$

where E is the energy density with respect to (z, θ, ψ). (The amount of energy between z and $z + \delta z$, with angle to the normal between θ and $\theta + \delta\theta$, and hitting the sides with horizontal angle between ψ and $\psi + \delta\psi$, is $E\,\delta z\,\delta\theta\,\delta\psi$.)

Now the rate of energy emission (density with respect to θ, ψ) from an area δS of the side (see Fig. 13) is $\alpha c\,\delta S \sin \theta \cos \psi$, where α is now a measure of the reflectivity of the surface: $\alpha = 1$ if it is perfectly black while $\alpha = 0$ for a perfect reflector. (The areas 'seen' by light travelling in direction with unit vector $\boldsymbol{q}$ is $-\delta S\,\boldsymbol{n}\cdot\boldsymbol{q}$.)

This is the power density with respect to solid angle. To obtain the density with respect to θ and ψ it must be multiplied by the usual $\sin \theta$. Moreover, integrating around the hole at a constant value of z (i.e. with respect to the polar angle ϕ; $\delta S = f\,\delta z\,\delta\phi$), gives a power emission, per unit length, of

$$2\pi\alpha c f \sin^2 \theta \cos \psi \ .$$

At the same time, whenever a light ray hits the side, it loses a proportion α of its energy into the body. The rate of number of reflections per unit time is

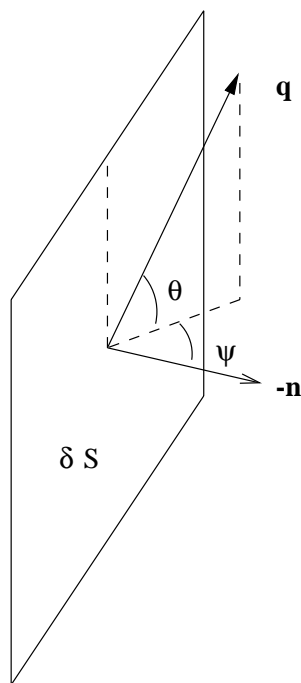$$\frac{dz}{dt}/dz = \frac{c}{2f} \sin \theta \sec \psi$$

Figure 13: Power emitted from the side of a hole.

so the rate of energy absorption is

$$\frac{\alpha c E}{2f} \sin\theta \sec\psi .$$

(In fact, α should probably depend upon the angle of incidence, *i.e.* on θ and ψ – and on the polarisation.) Combining these with (10),

$$\frac{\partial}{\partial z}(E\cos\theta) - \frac{f'}{f}\frac{\partial}{\partial\theta}(E\sin\theta) = 2\pi\alpha f \sin^2\theta\cos\psi - \frac{\alpha E}{2f}\sin\theta\sec\psi . \qquad (11)$$

For a significant absorption and emission over the depth of the pit, $\alpha = O(R/h)$, where R is again a typical size of f. With $\alpha \gg R/h$, the terms on the right-hand side of (11) dominate and

$$E \sim 4\pi f^2 \sin\theta\cos^2\psi . \qquad (12)$$

This expression is simply the distribution for black-body radiation. (This is as expected because for $\alpha = 1 \gg R/h$ the sides, as well as the bottom of the pit, are perfectly black.) This can be checked by rewriting the total energy density with respect to z and θ,

$$I = \int_0^f \int_0^{2\pi} \int_0^{2\pi} r\sin\theta \, d\varphi \, d\phi \, dr , \qquad (13)$$

22
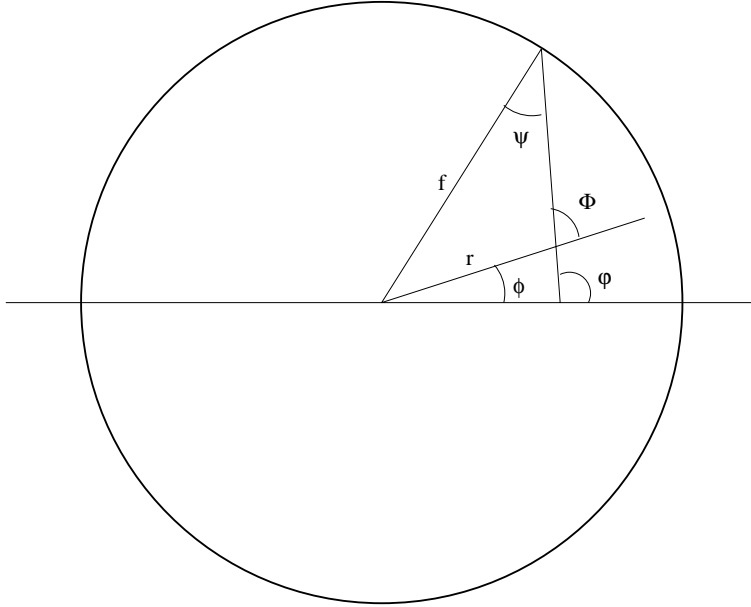
Figure 14: Angles and distances used in rewriting (13).

appropriately. First writing $\Phi = \varphi - \phi$ (see Fig. 14), the integral becomes

$$I = 2\pi \sin\theta \int_0^f \int_0^{2\pi} r \, d\Phi \, dr \; .$$

Then, using $\sin\psi / \sin\Phi = r/f$, and noting that for given r, $-\sin^{-1}(r/f) < \psi < \sin^{-1}(r/f)$,

$$
\begin{aligned}
I \;&= 4\pi f \sin\theta \int_0^f \int_0^{\sin^{-1} r/f} \frac{\cos\psi}{\cos\Phi} \, d\psi \, dr \\[2mm]
&= 4\pi f \sin\theta \int_0^{\pi/2} \int_{f\sin\psi}^f \frac{r\cos\psi}{\sqrt{(r^2 - f^2 \sin^2\psi)}} \, dr \, d\psi \\[2mm]
&= 4\pi f^2 \sin\theta \int_0^{\pi/2} \sin\theta \cos^2\psi \, d\psi \; ,
\end{aligned}
$$

using symmetry, changing the order of integration, and carrying out the r integration. Hence the black-body distribution (12) is recovered.

Of course (11) is a hyperbolic equation and to find the energy density E (and then the power distribution), its values should be given at places where the characteristics (as indicated by (9)) enter the region $0 < z < h$, $0 < \theta < \pi$ (see Fig. 15). ($\theta > \pi/2$ has to be included to allow for light coming down, as well as going up, the pit.) On $z = 0$, $0 < \theta < \pi/2$, E is just that for a black body (as this represents light coming from the black bottom of the pit), *i.e.* E is given by (12). For $z = h$, $\pi/2 < \theta < \pi$, E is fixed by the returning radiation (0 for "good" radiation in an ideal situation).
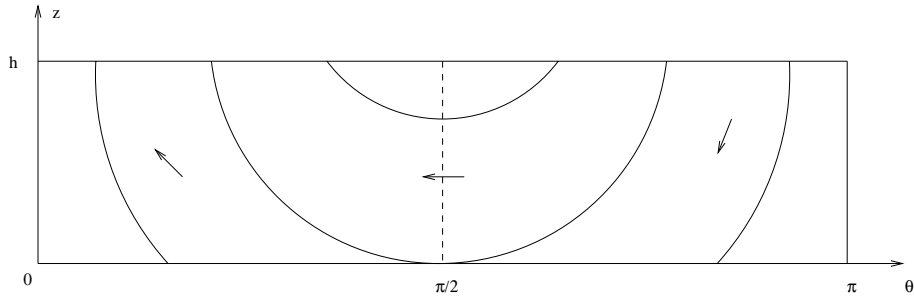
Figure 15: Characteristics in the $\theta - z$ plane for (11).

5   Possible Geometries and Difficulties

It appears from the work of the preceding section that possible devices might use radiators covered with small dimples. In particular, a radiator might be the outside of a circular cylinder, with a heat source inside, and a concentric cylinder with inward-facing TPV cells (Fig. 16(a)). Conversely, the cells could be arranged over the inner cylinder, with the outer cylinder as the radiator and the heat source beyond that (Fig. 16(b)). One slight variation on the small-hole approach was put forward. This would be to take the hole radius and spacing large enough for the useful radiation to exit normally from the surface but small enough for a significant proportion of the longer-wavelength light to be diffracted off in different directions (Fig. 16(c)). Of the two mentioned configurations, this might be thought to work better with the heat source surrounding the cells as now a significant part of the useless radiation misses the cells and return directly to the radiator (the shorter wavelengths still arriving perpendicularly at the cells). However, a significant proportion of this power now reaches the ends of the cylinders. Moreover, the diffracted light arriving at both the cells and the radiator does so with positive incident angle. For the cells, this means the filter has to cope with radiation incident with a variety of directions. The light reaching the radiator can be expected to be only partially absorbed by the black parts of the pits with most being reflected away again. In the absence of some other mechanism for removing the low-frequency light, this radiation will fill the space between the cells and emitter with approximately the black-body density corresponding to the temperature of the radiator.

This last problem will also tend to arise even with b large enough for diffraction to be negligible. Because the long-wavelength light will not be returned exactly along its original path, some proportion will be reflected again on its return to the radiating surface. This fraction could well be significant due to surface not being entirely covered with the pits. (Even light entering a pit can do so with too large an incident angle and would then be reflected back out rather than reach the end and get absorbed.) Supposing that the the rate at which the bad light is lost from directions corresponding to direct emission from and absorption by the pits into "off-normal" paths is β, the rate that the resulting "off-normal" light is returned to normal directions (and back into the pits) is also proportional to β, and the rate at which the off-normal light is lost to the outside world is proportional to γ, the intensity of the off-normal
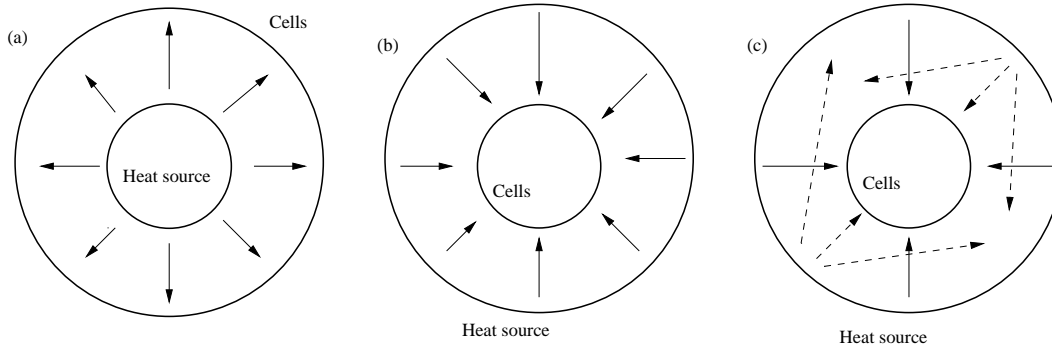
24

Figure 16: Possible geometries: (a) radiator inside receptors; (b) heat source surrounding cells; (c) $b \sim \lambda_b \gg \lambda_g$.
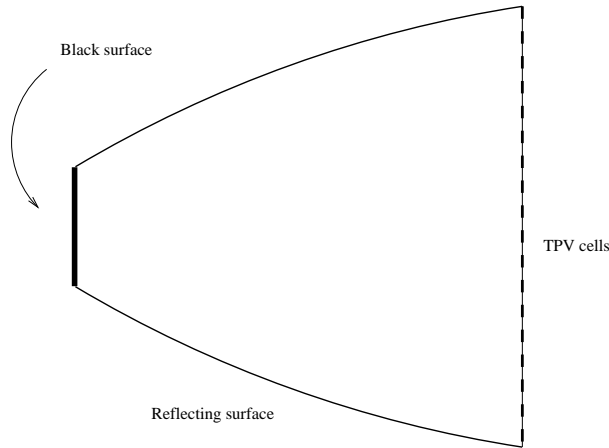

Figure 17: A single, large, light-emitting pit.

light will be $\beta/(\beta+\gamma)$. (For $\gamma = 0$ this intensity is 1, that is, the black-body level.) The total power loss is then proportional to $\beta\gamma/(\beta+\gamma)$; this would ideally be small.

One possible way of reducing this difficulty might be to have, instead of a surface with many small radiating pits and the TPV cells at some distance, one, or a few, large pit(s) with the cells across the opening(s) and arranged perpendicularly to the axis/axes (Fig. 17). Now any light reflected from the cells could return essentially along its original path.

Nomenclature

Other notation

A: complex amplitude of the magnetic field in positive z-direction.

a: radius of black body at bottom of pit.

$\boldsymbol{B}(\boldsymbol{x}, t)$: magnetic field.

b: radius of pit opening.

C: complex amplitude of the magnetic field in negative z-direction *or* arbitrary constant.

c: speed of light in medium.

$\boldsymbol{D}(\boldsymbol{x}, t)$: electric field.

$\boldsymbol{E}(\boldsymbol{x}, t)$: electric field.

$\tilde{\boldsymbol{E}}(\boldsymbol{x})$: time-independent part of electric field.

$F(\cdot)$: arbitrary function.

$f(\cdot)$: function describing side surface of pit.

$\boldsymbol{H}(\boldsymbol{x}, t)$: magnetic field.

h: depth of pit.

K: dimensionless wave number, value $K = kh$.

k: wave number.

$\boldsymbol{q}(\boldsymbol{x}, t)$: power density.

R: typical pit radius.

δS: differential area element on side of pit.

t: time.

$U(\cdot)$: coordinate of plane wave solution.

$u(\cdot)$: arbitrary coordinate of $\tilde{\boldsymbol{E}}$ in scaled coordinate system.

x: direction along radiator.

y: direction along radiator.

$\mathcal{Z}$: the integers.

Z: scaled direction normal to radiator, value z/h.

z: direction normal to radiator.

α: angle of incidence of plane wave *or* angle of side wall of pit *or* measure of reflectivity of surface.

β: angle of transmitted plane wave *or* rate at which off-normal light is lost from pits to reabsorption.

γ: angle of reflected plane wave *or* rate at which off-normal light is lost from pits to outside environment.

δ: small parameter.

ϵ: electrical permittivity.

ζ: scaled variable, defined as z/R.

η: stretched variable, defined as $\delta\rho$.

θ: angle of incidence of light ray.

λ: wavelength of light.

μ: magnetic permeability.

ν: arbitrary parameter.

ξ: stretched variable, defined as δZ.

ρ: scaled radial coordinate, value $r/\sqrt{\lambda h}$.

$\Phi(\xi, \eta)$: coefficient in solution for U *or* $\varphi - \phi$.

φ: azimuthal angle in spherical coordinates.

ϕ: azimuthal angle in cylindrical coordinates.

$\Psi(\xi, \eta)$: exponent in solution for U.

ψ: horizontal angle of reflection.

Ω: solid angle.

ω: frequency of plane wave.

Other notation

1: as a subscript on ψ, used to indicate an incidence angle.

a: as a subscript, used to indicate one medium in an interface problem.

b: as a subscript, used to indicate one medium in an interface problem.

g: as a subscript, used to indicate the cutoff between useful and useless light.

I: as a subscript, used to indicate an incident wave.

$j \in \{1, 2, 3\}$: as a subscript, used to indicate the x-, y-, and z-coordinates of a vector function.

$j \in \mathcal{Z}$: as a subscript, used to indicate a medium in a multiple-reflection problem.

R: as a subscript, used to indicate a reflected wave.

T: as a subscript, used to indicate a transmitted wave.

References

[1] C.M. Cornelius & J.P. Dowling, *Modification of Planck blackbody radiation by photonic band-gap structures*, Phys. Rev. A, **59**,1999, 4736–4746.

[2] M. Perlmutter & J. R. Howell, *A strongly directional emitting and absorbing surface*, ASME Jl. Heat Transfer, **85**, 1963, 282–283.

[3] H. Masuda, *Directional control of radiation heat transfer by V-groove cavities – collimation of energy in direction normal to cavity opening*, ASME Jl. Heat Transfer, **102**, 1980, 563–567.

[4] J. C. Engineer, J. R. King, & R. H. Tew, *Diffraction by slender bodies*, Eu. Jl. Appl. Maths., **9**, 1998, 129–158.
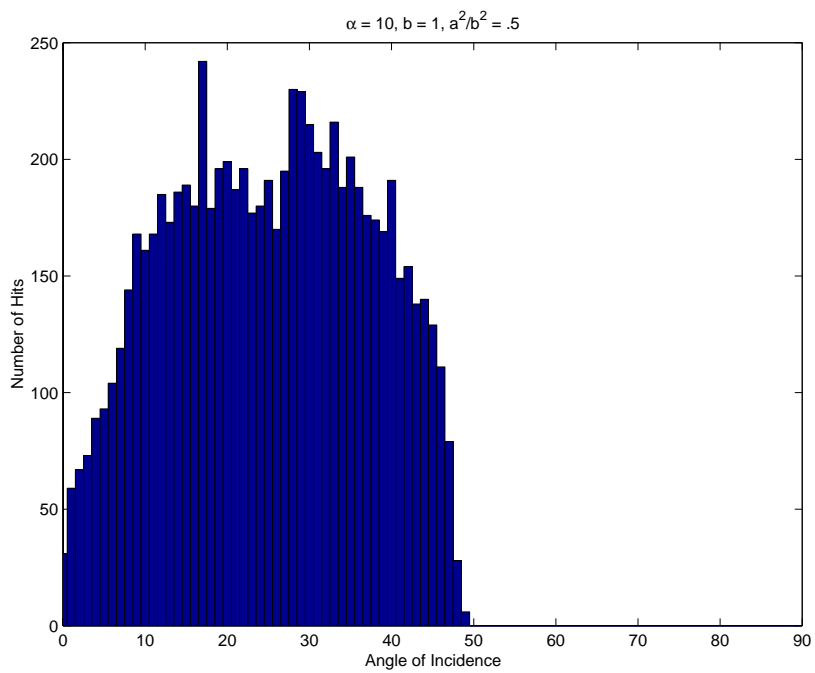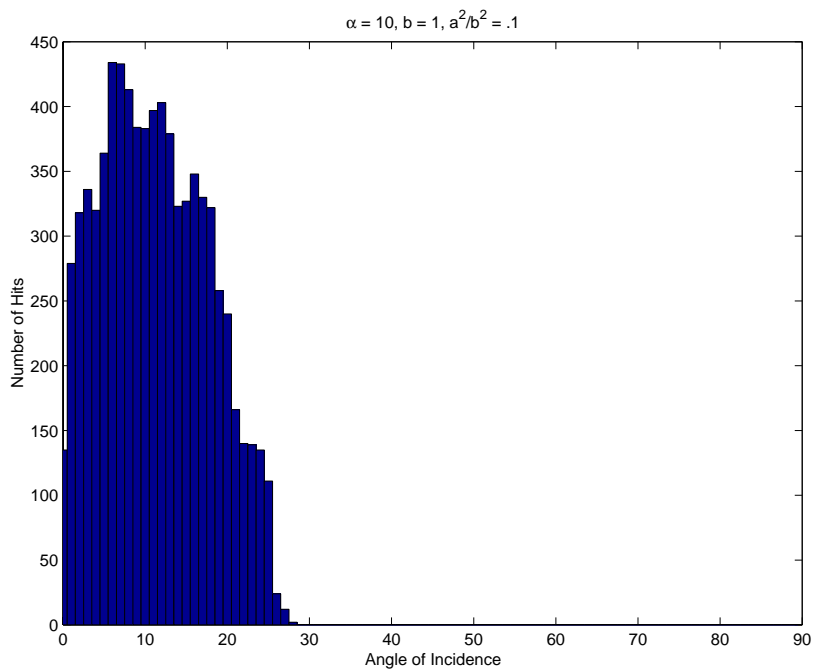
Power distributions from Monte-Carlo simulations
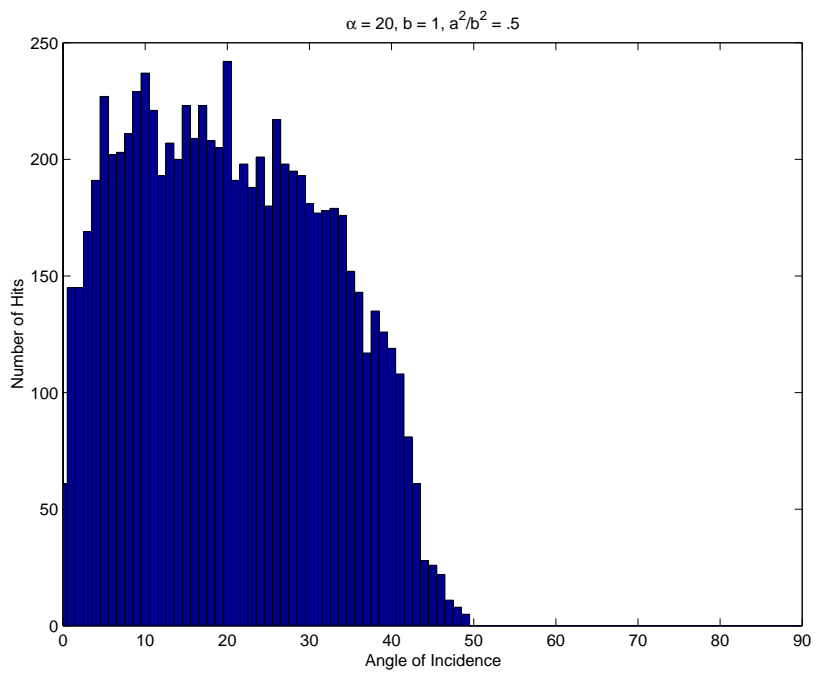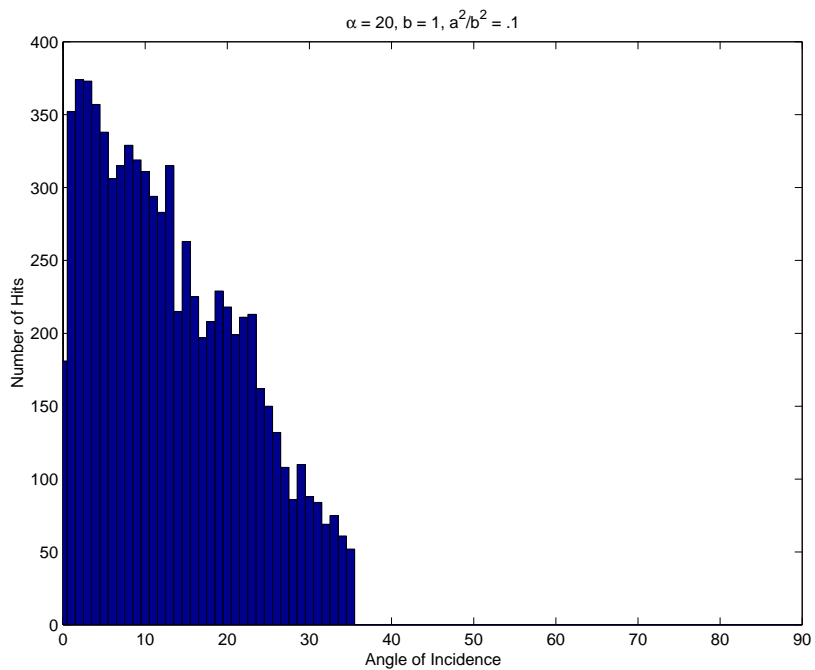
The following are:

1. a check with the plane using a two-dimensional calculation

2–5. four two-dimensional simulations (wedges)
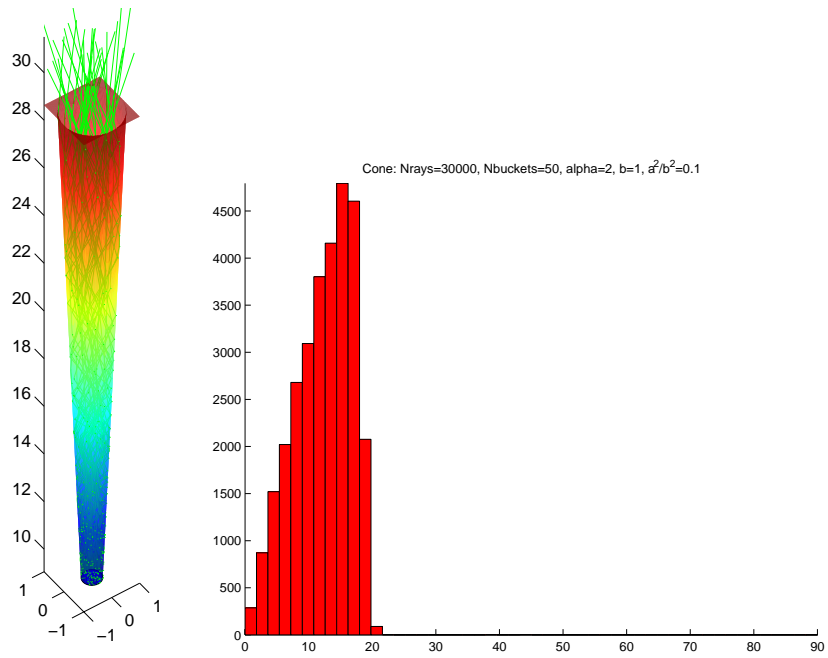
6–9. four three-dimensional simulations (frusta).
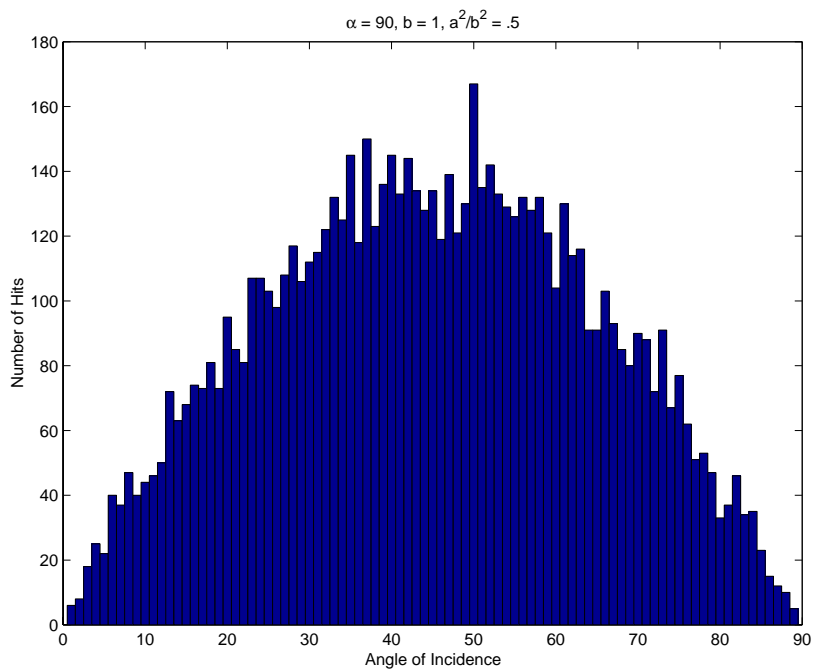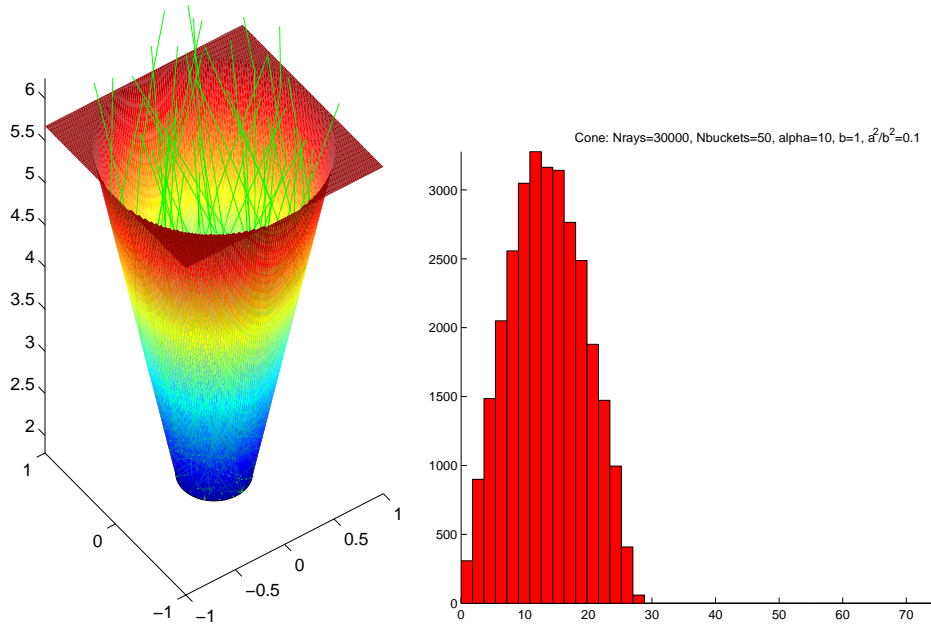
Check with the plane (wedge with $\alpha = 90^\circ$).

Two-dimensional wedges with $\alpha = 10\,^{\circ}$.
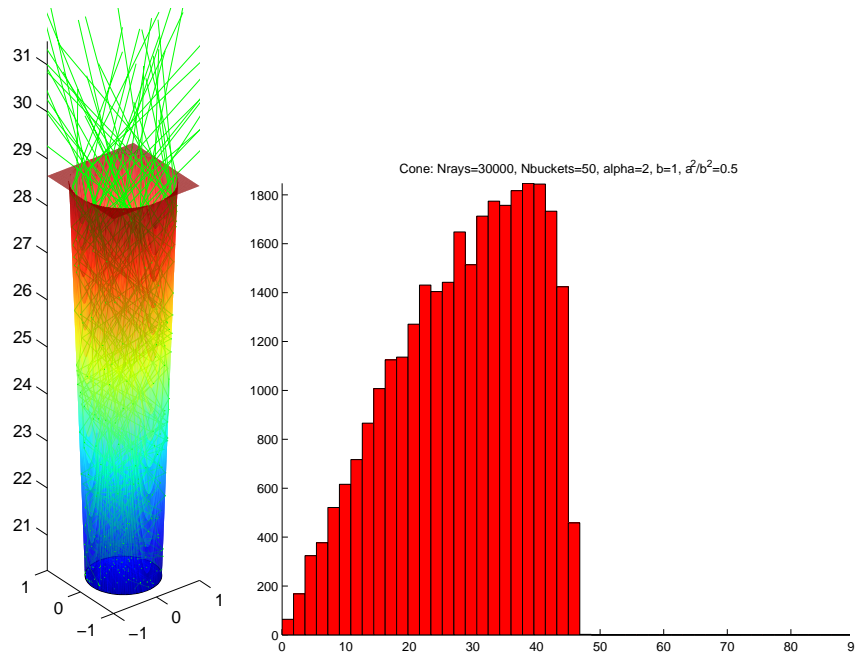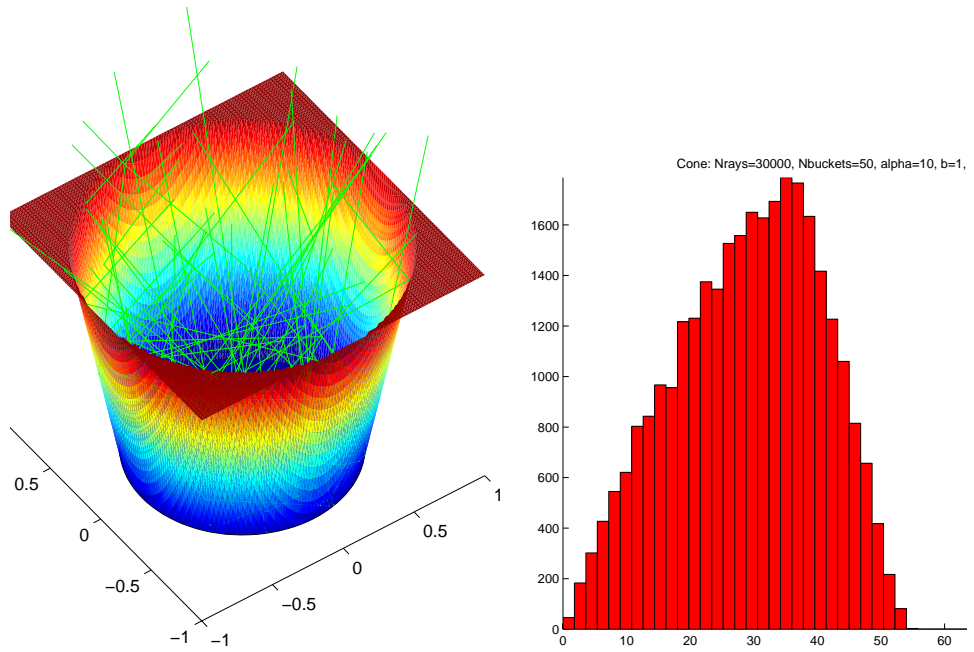
Two-dimensional wedges with $\alpha = 20\,^\circ$.

Three-dimensional frustum with $\alpha = 2°$ and $a^2/b^2 = 0.1$.

Three-dimensional frustum with $\alpha = 10°$ and $a^2/b^2 = 0.1$.

Three-dimensional frustum with $\alpha = 2°$ and $a^2/b^2 = 0.5$.

Three-dimensional frustum with $\alpha = 10°$ and $a^2/b^2 = 0.5$.